



Earing prediction performance of homogeneous polynomial-based yield function coupled with the combined hardening model for anisotropic metallic materials

Homojen polinom tabanlı akma fonksiyonunun birleşik pekleşme modeli ile kullanımının anizotropik metalik malzemeler üzerindeki kulaklanma tahmin performansı

Toros Arda AKŞEN¹, Murat ÖZSOY¹, Mehmet FIRAT^{1*}

¹Department of Mechanical Engineering, Faculty of Engineering, The University of Sakarya, Sakarya, Turkey.
ardaaksen@sakarya.edu.tr, ozsoy@sakarya.edu.tr, firat@sakarya.edu.tr

Received/Geliş Tarihi: 09.08.2022
Accepted/Kabul Tarihi: 20.02.2023

Revision/Düzelme Tarihi: 14.02.2023

doi: 10.5505/pajes.2023.79804
Research Article/Araştırma Makalesi

Abstract

In the cup drawing process, the tensile stress in the radial direction is dominant during the drawing. However, the sheet bends around the punch and die radiuses, and the fibers touching the punch and die are exposed to compression, while the outer surfaces are exposed to tension. Therefore, the stress state at the radius regions of punch and die becomes complicated to overcome due to the bending and may influence the final earing form. The present study investigates the influence of a plasticity model involving an advanced yield criterion coupled with a combined hardening model on the earing prediction in the cup drawing process of AA6016-T4 aluminum alloy. Therefore, isotropic hardening and combined hardening models are implemented, respectively so as to show the kinematic hardening effect on the earing prediction performance. The combined hardening model comprises Armstrong-Frederic kinematic hardening and isotropic hardening rules together to characterize the hardening behavior of the sheet, and the parameters of the hardening model were obtained by considering a reversal shear test. A sixth-order polynomial-based yield criterion was implemented to represent the anisotropic response of the sheet successfully. The Hill48 yield criterion was also considered in the present study for comparison purposes. The analyses were conducted based on the additive plasticity approach and using the implicit stress update scheme in Marc commercial software. The punch force-displacement responses and earing profile predictions were obtained numerically and compared with the experimental outcomes. It was seen that introducing the combined hardening model enhances the earing prediction capability for both yield criteria. With the incorporation of the combined hardening rule, the improvement in the prediction of the earing profile was more apparent in HomPol6 results compared to Hill48. The HomPol6 yield criterion coupled with the combined hardening rule led to a better agreement in the prediction of ear formation.

Keywords: Cup drawing, Earing, Kinematic hardening, Plasticity.

Öz

Kap çekme işlemi esnasında, radyal yön boyunca çekme gerilmesi mevcuttur. Bununla birlikte şekillendirilecek sac, zımba ve kalıp köşelerinin etrafında bükülmektedir ve köşelere temas eden iç yüzeyler basma gerilmesi etkisi altındayken, dış yüzeyler ise çekme etkisi altındadır. Bu durum sacın zımba ve kalıp köşelerinde bükülen bölümlerindeki gerilme durumunu karmaşık bir hale getirmektedir ve nihai kulak formunu etkileyebilmektedir. Bu çalışma, gelişmiş bir akma fonksiyonu ve bir birleşik pekleşme modeli içeren bir plastisite modelinin kulaklanma tahmin performansını incelemektedir. Bu kapsamda AA6016-T4 alüminyum alaşımının derin çekme işlemi incelenmiştir. Birleşik pekleşme modelinin kulaklanma tahmin performansına etkisini daha net ortaya koymak amacıyla, izotropik ve birleşik pekleşme kuralları ayrı ayrı analizlere entegre edilmiştir. Malzemenin pekleşme davranışını tanımlamak amacıyla kullanılan birleşik pekleşme modeli, Armstrong-Frederic kinematik pekleşme ve izotropik pekleşme modellerinin birleşimidir ve birleşik pekleşme modelinin parametreleri bir tersinir kayma testinin verileri kullanılarak elde edilmiştir. Sacın anizotropik davranışını isabetli bir şekilde tanımlamak amacıyla altıncı dereceden homojen polinom tabanlı bir akma fonksiyonu kullanılmıştır. HomPol6 kriterinin tahmin performansını göstermek için simülasyonlar Hill48 akma kriteri kullanılarak da yürütülmüştür. Simülasyonlar Marc ticari yazılımında eklemeli plastisite yaklaşımı ve kapalı zaman adımı gerilme güncelleme şeması kullanılarak yürütülmüştür. Zımba kuvvet-deplasman davranışları ve kulak profil tahminleri sayısal olarak elde edilmiş ve deneysel sonuçlarla kıyaslanmıştır. Birleşik pekleşme modelinin kulaklanma tahmin yeteneğini iki akma kriteri için de iyileştirdiği görülmüştür. Bu iyileşmenin HomPol6 sonuçları için daha belirgin olduğu da kaydedilmiştir. En iyi kulak oluşum tahmininin, HomPol6 akma kriteri ile birleşik pekleşme kuralı kullanıldığında gerçekleştiği görülmüştür.

Anahtar kelimeler: Kap çekme, Kulaklanma, Kinematik pekleşme, Plastisite.

1 Introduction

Earing defect is a fundamental issue observed in the cup drawing process. The ears should be trimmed after the deformation, and this process not only decreases the production rate but also leads to material loss [1]. Therefore, prediction and prevention of the earing defect become an essential topic, especially in the automotive industry. Although the finite element (FE) method is a practical approach for

predicting the earing defect, an advanced plasticity model is required. Earing is mainly due to the anisotropy-based uneven material flow into the die cavity. However, characterizing the texture effect may not be adequate for the earing defect prediction. Bending-unbending issues observed at the punch and die radiuses may also influence the cup height [2]. Consequently, an anisotropic yield criterion coupled with a combined hardening rule is recommended to predict ear formation.

*Corresponding author/Yazışılan Yazar

The studies carried out in the past concentrated on the effect of the yield criteria. Chung and Shah [2] performed FE simulations of the cup drawing test and bulge test of AA2008-T4. Since the cup drawing process includes compression, tension, stretching, bending, and unbending conditions, they used tensile test and compression test data and considered the average of these two data for the yield criterion calibration. Yld91 criteria were implemented, and it is reported that good approximations were obtained. Yoon et al. [3] investigate the influence of the yield surface shape and the translation of the yield surface center on the earing defect prediction of AA2008-T4 alloy by implementing the Yld96 yield criterion. They pointed out that both shape and the center translation of the yield surface are essential in predicting ear formation. Yoon et al. [4] and Yoon et al. [5] conducted similar studies for the earing prediction of AA2090-T3 aluminum alloys using different yield criteria. The importance of the yield criterion and the back stress translation was emphasized. Yoon et al. [6] performed the FE simulations of AA5042-H2 alloy using CPB06ex2 and Yld2000-2D yield criteria. Yld2000-2D could not capture the correct numbers of ears, while CPB06ex2 could predict the actual ear numbers. Thus, the importance of the yield criterion was also put forward for highly anisotropic materials. Vladimirov et al. [7] implemented the multiplicative decomposition formulations based on the deformation gradient's disintegration into elastic and inelastic parts. They adopted the Hill48 yield criterion to predict the earing behavior of two different aluminum alloys. Chatti and Chtioui [8] implemented the Hill48 yield criterion coupled with the kinematic hardening rule to estimate the earing profile of the AA2090-T3 alloy. They pointed out that the prediction performance was improved when the kinematic hardening rule was assumed. Vrh et al. [9] implemented the BBC2008 yield criterion with the next increment corrects error method to predict the earing defects of AA5042-H2 and AA2090-T3 aluminum alloys. The constitutive model was found to be potent for highly anisotropic materials. Park and Chung [10] performed numerical analyses of the cup drawing process with Hill48 and Yld2000-2d criteria. They adopted the associated flow rule (AFR) for AA2090-T3 and AA5042 aluminum alloys exhibiting 6 and 8 ears, respectively, in physical processes. Yld2000-2d criterion along with the AFR provides good approximations with the experiments. Othmen et al. [11] evaluated the effects of work hardening and anisotropy on the strain distribution and the punch force-displacement prediction accuracy in the reverse deep drawing process. They employed Mises and Hill48 yield criteria, coupled with isotropic and combined hardening rules. For the first stage of the drawing, the punch force response was predicted by all the plasticity models. For the second stage, the punch force evolution was found to be dependent on the yield locus definition, while the strain distribution was emphasized to be affected by the hardening behavior. Grillo et al. [12] proposed new stress update algorithm schemes for backward Euler and forward Euler approaches separately to enhance the earing prediction performance and decrease the solution times. They compared the results with the classical approaches and obtained good agreements. Izadpanah et al. [13] conducted a similar study on AA3105 aluminum alloy by implementing Hill48 and BBC2003 criteria, and they emphasized the influence of the yield function. Singh et al. [14] conducted similar research on the commercially pure titanium sheets, which have high r values. The researchers used the CPB06 yield criterion and performed an optimization study on the blank's shape to minimize the earing and material loss. Feng et al. [15]

developed a micromechanical constitutive model that contains a back stress definition at the slip system level to predict the earing defect of the AA6022-T4 aluminum alloy. They also implemented a macro-mechanic homogeneous anisotropic hardening model and compared the numerical results in between. It was indicated that the developed micromechanical model led to more computational cost, while the micromechanical model had lower CPU solution times. Recently, Habraken et al. [16] extensively investigated several parameters, including the yield criteria, flow rule, hardening rule, friction, stress update schemes, etc., on the earing prediction performance. Kim et al. [17] conducted a study adopting Hill48 and Yld2000-2d yield criteria for predicting the earing phenomenon in the cup drawing process of commercially pure titanium. They also assessed the influence of the associated and non-associated flow rules. It was concluded that the evolution of the yield potential had a noticeable effect on the earing profile.

The literature studies were generally concentrated on the impact of the yield criteria on the prediction of ear formation. Capturing the ear location is associated with the r value predictions, while the magnitude of the ears can only be captured by the criteria predicting the directionalities of yield stress ratios. Therefore, the yield criterion is expected to capture both the r value and yield stress ratio directionalities for improved earing prediction performance. However, different parameters may affect the earing prediction performance. Although several studies emphasized the translation of the yield surface [3]-[5],[7],[11], in general, the isotropic hardening rule was assumed for the sake of simplicity. The effect of the hardening rule was generally disregarded. In the deep drawing process, the bending-unbending issue on the die radius and the reverse bending-unbending issue on the punch radius were taken place [18],[19]. The Bauschinger effect is induced along these regions due to the reversed loading paths. Moreover, the transient behavior that is observed under the reversal loading may also affect the earing defect since the sheet metal is fully drawn over the punch and die corners. Considering these conditions at the corners of the punch and die, the hardening rule may have a significant role. The combined hardening rule regards the yield surface motion and the expansion together. In reversal loadings, the Bauschinger effect or transient behavior may only be characterized by the kinematic hardening part of the combined hardening rule. In the past, linear [20],[21], multilinear [22]-[24], and nonlinear [25], [26] hardening rules were introduced.

In this study, the cup drawing operation of an anisotropic metallic material, namely AA6016-T4 alloy, was simulated by adopting the sixth-order polynomial yield criterion (HomPol6) and Hill48 criterion coupled with a combined hardening model. HomPol6 criterion has 16 coefficients to adjust and provides the high prediction performance anisotropic features. Moreover, biaxial yield stress and r value were also predicted by HomPol6. The combined hardening effect was implemented into the main plasticity model so as to enhance the prediction performance. Therefore, the behaviors stimulated by the reversal loading situations on the radius regions were considered for the earing phenomenon. The Armstrong-Frederic model represented the kinematic part of the combined hardening rule. To show the pure performance of the implemented hardening rule, the analyses were carried out based on considering only the expansion of the yield surface and both enlargement and translation of the yield surface

center, separately. The analyses were conducted adopting the backward Euler stress update scheme (Implicit) and based on the co-rotational plasticity approach in the Marc software. A user-defined material subroutine called Hypela2 was employed in the simulations. The numerical punch force – stroke and earing prediction results were obtained for both cases and compared with the experimental results.

This study consists of 6 sections. In section 2, the benchmark model and the experimental procedures were explained, and the mechanical properties of AA6016-T4 aluminum alloy were presented. In section 3, the HomPol6 yield criterion, hardening rule, and the AFR used in this study were explained. In section 4, calculated anisotropy parameters and the performance of the yield criterion were presented. Identification of the combined hardening rule parameters was also explained in this section. Section 5 gives information about the FE model of cup drawing and simulation results. In section 6, conclusions were summarized.

2 Mechanical tests

This section gives information about the experimental procedure of the benchmark study on AA6016-T4 aluminum alloy sheet having 0.98 mm thickness [16]. The uniaxial tensile tests were conducted in seven directions, from the rolling direction to the transverse direction, with intervals of 15° degrees at the Tokyo University of Agriculture and Technology. Conventional uniaxial tensile test specimens (The gauge length and width are 50 mm and 12.5 mm, respectively) were used. The tests were carried out at a constant speed of 10⁻³ s⁻¹, and a mechanical extensometer was used for sensitive strain measurement. In addition, the biaxial yield stress and procured from the biaxial tensile test in compliance with the ISO 16842 standards conducted on cruciform specimens. The test standards and the geometry of the test specimens were explained elaboratively in ref [16]. Within the scope of this study, the uniaxial tensile test data was utilized so as to obtain the hardening parameters and the yield function calibration of the material. Table 1 shows the experimental r-value, yield stress directionalities, and the biaxial data.

Table 1. Anisotropic properties of AA6016-T4 alloy [16].

θ	0	15	30	45
r_θ	0.526	0.344	0.301	0.253
σ_θ/σ_0	1	0.944	0.913	0.908
θ	60	75	90	Biaxial
r_θ	0.294	0.393	0.601	0.854
σ_θ/σ_0	0.898	0.928	0.983	0.991

The combined hardening model parameters were obtained from the reversal shear test conducted by the University of Aveiro. These data were also provided by the ESAFORM 2021 benchmark organizing team [16]. The reversal shear test data performed in RD was considered as reference data. Single element simulations were considered for the combined hardening parameter's determination, and the inverse method was adopted. As the main issue, a cup drawing process of the AA6016-T4 alloy was carried out. Figure 1 demonstrates the dimensions of the ESAFORM 2021 benchmark cup drawing process tools.

The diameter of the blank sheet was 107.54 mm. The sheet was subjected to a clamping force of 40 kN during the deformation. The rigid body stoppers were used to block the blank holder when the blank's periphery reached the cup wall region. The

drawing operation was suspended when the punch moved 54 mm vertical distance.

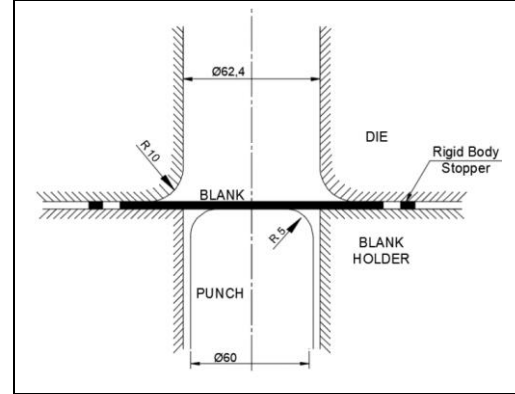


Figure 1. A schematic view of the cup drawing process [16].

3 Plasticity model

The information relevant to the implemented plasticity model comprises the HomPol6 yield criterion, the AFR, and the hardening rule. The additive plasticity approach was implemented in the numerical simulations. According to this approach, the incremental strain can be resolved into recoverable and irrecoverable components. (Eq. (1)).

$$d\varepsilon_{ij} = d\varepsilon_{ij}^e + d\varepsilon_{ij}^p \quad (1)$$

Incremental elastic strain involves the deviatoric and hydrostatic parts (Eq. (2)) [27], while the plastic strain increment is purely deviatoric ($d\varepsilon_{ij}^p = de_{ij}^p$).

$$d\varepsilon_{ij}^e = de_{ij}^e + d\varepsilon_m I \quad (2)$$

Where, e_{ij} refers to the deviatoric component of strain, ε_m is the hydrostatic component of strain, and I is the Kronecker delta. Similarly, stress increment comprises of the deviatoric part (S_{ij}) responsible for the shape change and the hydrostatic part (σ_m) responsible for the volume change.

$$d\sigma_{ij} = dS_{ij} + d\sigma_m I \quad (3)$$

A correlation between the incremental deviatoric strain and the deviatoric stress can be established in Eq. (4).

$$dS_{ij} = 2Gde_{ij}^e \quad (4)$$

Where, G is the shear modulus. In three-dimensional stress space, the yield criterion defines the boundary at which the plastic flow initiates (Eq. (5)).

$$f = \sigma_{eqv}(S_{ij} - \alpha_{ij}) - \sigma_0(\varepsilon_{eqv}^p) = 0 \quad (5)$$

Where the α_{ij} represents the motion of the yield surface. In the present work, two different yield criteria, namely Hill48 and HomPol6, are implemented into the Marc software to evaluate the effect of the yield surface definition coupled with the combined hardening rule on the earing defect. Hill48 (Eq. (6)) is the first anisotropic yield criterion proposed [28].

$$2f_{Hill48} = F(\sigma_{yy} - \sigma_{zz})^2 + G(\sigma_{zz} - \sigma_{xx})^2 + H(\sigma_{xx} - \sigma_{yy})^2 + 2L\tau_{yz}^2 + 2M\tau_{zx}^2 + 2N\tau_{xy}^2 = 1 \quad (6)$$

Where F, G, H, L, M and N are the anisotropy constants. The F, G, H, and N parameters were obtained by utilizing the following equations.

$$F = \frac{r_0}{r_{90}(1 + r_0)} \quad (7)$$

$$G = \frac{1}{1 + r_0} \quad (8)$$

$$H = \frac{r_0}{1 + r_0} \quad (9)$$

$$N = \frac{(r_0 + r_{90})(1 + 2r_{45})}{2r_{90}(1 + r_0)} \quad (10)$$

The first polynomial yield criterion was introduced by Gotoh [29]. The polynomial-based functions have a simple form that makes the direction of the plastic flow straightforward. This criterion has nine coefficients to be calibrated analytically; however, it could not produce a convex yield surface for all the materials. Later, Soare [30], [31] improved the identification procedure of Gotoh's criterion to produce a convex yield locus through the optimization steps for some anisotropy parameters. Moreover, Soare [30] introduced the sixth-order homogeneous polynomial-based yield function (Eq. (11)) that has 16 parameters. The high number of parameters provides better prediction performance of the anisotropy directionalities.

$$\begin{aligned} f_{HomPol6} = & (c_1\sigma_{xx}^6 + c_2\sigma_{xx}^5\sigma_{yy} + c_3\sigma_{xx}^4\sigma_{yy}^2 \\ & + c_4\sigma_{xx}^3\sigma_{yy}^3 + c_5\sigma_{xx}^2\sigma_{yy}^4 \\ & + c_6\sigma_{xx}\sigma_{yy}^5 + c_7\sigma_{yy}^6 \\ & + (c_8\sigma_{xx}^4 + c_9\sigma_{xx}^3\sigma_{yy} + c_{10}\sigma_{xx}^2\sigma_{yy}^2 \\ & + c_{11}\sigma_{xx}\sigma_{yy}^3 + c_{12}\sigma_{yy}^4)\sigma_{xy}^2 \\ & + (c_{13}\sigma_{xx}^2 + c_{14}\sigma_{xx}\sigma_{yy} \\ & + c_{15}\sigma_{yy}^2)\sigma_{xy}^4 + c_{16}\sigma_{xy}^6)^{\frac{1}{6}} - \sigma_0 \end{aligned} \quad (11)$$

The parameters c_1 , c_2 , c_6 , and c_7 are analytically calibrated through the Eq. (7-10). Here c_1 and c_7 can be computed considering the yield condition in RD and TD, respectively. In a similar manner, c_2 and c_6 are identified based upon the r values in RD and TD.

$$c_1 = 1 \quad (12)$$

$$c_7 = \left(\frac{\sigma_0}{\sigma_{90}}\right)^6 \quad (13)$$

$$c_2 = \frac{-6r_0}{(1 + r_0)} \quad (14)$$

$$c_6 = \frac{-6r_{90}c_7}{(1 + r_{90})} \quad (15)$$

Other HomPol6 parameters cannot be calculated by explicit equations. Hence, these parameters were computed by employing the least square optimization procedure. This method regards the difference between the square values of the analytical predictions and the experimental equivalents of the anisotropy features (Eq. (16)). Four different weigh functions (w_m for yield stress ratio directionality, w_n for r value directionality, w_k and w_l for biaxial data) were assigned for each anisotropy feature in order to regulate the influence of

each feature, separately. Thus, it is aimed to minimize the errors.

$$\begin{aligned} H = & \sum_m w_m \left(\frac{(\sigma_\theta)_m^{pr}}{(\sigma_\theta)_m^{exp}} - 1\right)^2 + \sum_n w_n \left(\frac{(r_\theta)_n^{pr}}{(r_\theta)_n^{exp}} - 1\right)^2 \\ & + \sum_k w_k \left(\frac{(\sigma_b)_k^{pr}}{(\sigma_b)_k^{exp}} - 1\right)^2 \\ & + \sum_l w_l \left(\frac{(r_b)_l^{pr}}{(r_b)_l^{exp}} - 1\right)^2 \end{aligned} \quad (16)$$

In Eq. (11), θ represents the material's orientation in which the yield stress ratio and the r value are numerically predicted or experimentally measured. The subscript "b" represents biaxial data. The uniaxial tensile tests in different material orientations should be carried out up to a specific strain value in order to measure the experimental r values. In this study, these values were measured at a displacement value corresponding to the plastic strain value of 0.1 [16]. The r value in an arbitrary θ orientation can be obtained by Eq. (17).

$$r_\theta = \frac{d\varepsilon_w}{d\varepsilon_t} \quad (17)$$

The bulge test or the tensile test of the cruciform sample should be performed to obtain the biaxial r value. Then the biaxial r value is calculated by the following equation.

$$r_b = \frac{d\varepsilon_{yy}}{d\varepsilon_{xx}} \quad (18)$$

The stress taking place in the orientation of θ angle can be disintegrated into the components as in Eq. (19-21).

$$\sigma_{xx} = \sigma_\theta \cos^2\theta \quad (19)$$

$$\sigma_{yy} = \sigma_\theta \sin^2\theta \quad (20)$$

$$\sigma_{xy} = \sigma_\theta \cos\theta \sin\theta \quad (21)$$

Normalized yield stress and the r value along an arbitrary orientation are predicted using Eq. (22) and (23) based on the above stress components.

$$\sigma_\theta^{pr} = \frac{\sigma_0}{f_{HomPol6}(\sigma_{xx} = \cos^2\theta, \sigma_{yy} = \sin^2\theta, \sigma_{xy} = \cos\theta \sin\theta)} \quad (22)$$

$$\begin{aligned} r_\theta^{pr} = & \frac{d\varepsilon_{\theta(width)}^{pr}}{d\varepsilon_{\theta(thickness)}^{pr}} \\ = & \frac{d\varepsilon_{xx}^p \sin^2\theta + d\varepsilon_{yy}^p \cos^2\theta - d\varepsilon_{xy}^p \cos\theta \sin\theta}{-(d\varepsilon_{xx}^p + d\varepsilon_{yy}^p)} \end{aligned} \quad (23)$$

The AFR is adopted in this work, and this rule determines the direction of the incremental plastic strain. The AFR is expressed in Eq. (24).

$$d\varepsilon_{ij}^p = d\lambda \frac{df}{d\sigma_{ij}} \quad (24)$$

Where $d\lambda$ is the proportionality factor, f denotes the plastic potential and $d\varepsilon_{ij}^p$ refers to the increment of plastic strain [32]. Considering the Eq. (24), the Eq. (23) can be written as follows.

$$= \frac{\frac{\partial f_{HomPol6}}{\partial \sigma_{xx}} \sin^2 \theta + \frac{\partial f_{HomPol6}}{\partial \sigma_{yy}} \cos^2 \theta - \frac{\partial f_{HomPol6}}{\partial \sigma_{xy}} \cos \theta \sin \theta}{-\left(\frac{\partial f_{HomPol6}}{\partial \sigma_{xx}} + \frac{\partial f_{HomPol6}}{\partial \sigma_{yy}}\right)} r_{\theta}^{pr} \quad (25)$$

Similarly, biaxial yield stress and r value data predictions are given in Eq. (26) and (27).

$$\sigma_b^{pr} = \frac{\sigma_0}{f_{HomPol6}(\sigma_{xx} = \sigma_b, \sigma_{yy} = \sigma_b, \sigma_{xy} = 0)} \quad (26)$$

$$r_b^{pr} = \frac{\frac{\partial f_{HomPol6}}{\partial \sigma_{xx}}(\sigma_{xx} = \sigma_b, \sigma_{yy} = \sigma_b, \sigma_{xy} = 0)}{\frac{\partial f_{HomPol6}}{\partial \sigma_{yy}}(\sigma_{xx} = \sigma_b, \sigma_{yy} = \sigma_b, \sigma_{xy} = 0)} \quad (27)$$

In this work, Armstrong – Frederic (A-F) type hardening model that is given in Eq. (28) is used to describe the evolution of the back stress curve [25].

$$d\alpha_{ij} = \frac{2}{3} C d\varepsilon_p - \gamma \alpha_{ij} dp \quad (28)$$

Where the tensor α_{ij} represents the displacement of the yield surface's center, C and γ are the adjustable material constants. The first term in Eq. (28) characterizes the linear part of the back stress in analogy to Prager's rule, while the second term represents the fading dynamic memory [33],[34]. Correlatively, the back stress curve saturates at the value of C/γ . dp is the equivalent plastic strain that is expressed in Eq. (29).

$$dp = \sqrt{\frac{2}{3} de^p : de^p} \quad (29)$$

4 Material characterization

This section provides information on the analytical predictions of the Hill48 and HomPol6 yield functions. These analytical predictions include the comparative r value, normalized yield stress directionalities, and the yield surface boundaries in the principal stress frame. Hill48 criterion was adopted only for comparison purposes. Furthermore, the identification procedures of the isotropic hardening, the combined isotropic-kinematic hardening rule parameters as well as the produced hardening curves were presented.

The parameters of Hill48 and HomPol6 criteria are summarized in Table 2 and 3, respectively.

Table 2. Hill48 coefficients for AA6016-T4.

F	G	H	L	M	N
0.574	0.65	0.345	1.500	1.500	0.9

Table 3. HomPol6 coefficients for AA6016-T4.

C ₁	C ₂	C ₃	C ₄
1.00	-2.068	3.532	-3.931
C ₅	C ₆	C ₇	C ₈
3.911	-2.496	1.108	16.412
C ₉	C ₁₀	C ₁₁	C ₁₂
-7.217	11.926	-5.02	18.23
C ₁₃	C ₁₄	C ₁₅	C ₁₆
22.47	17.981	24.432	13.931

The analytical predictions of the Hill48 and HomPol6 yield criteria are illustrated comparatively in Figure 2 (for constructed yield loci) and Figure 3 (for directional dependencies of r value and yield stress ratio).

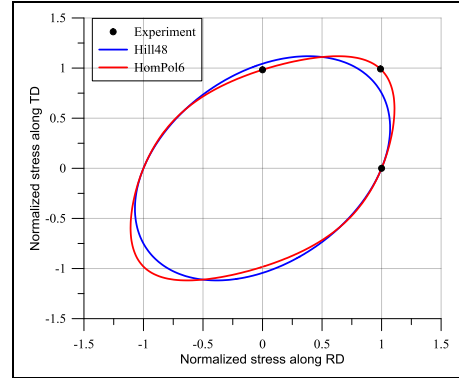
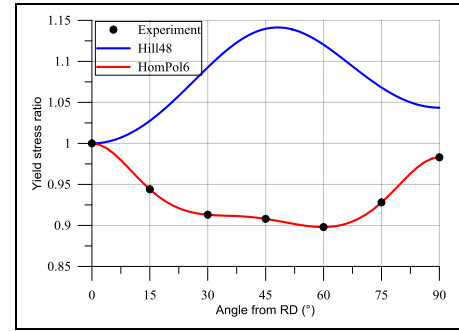
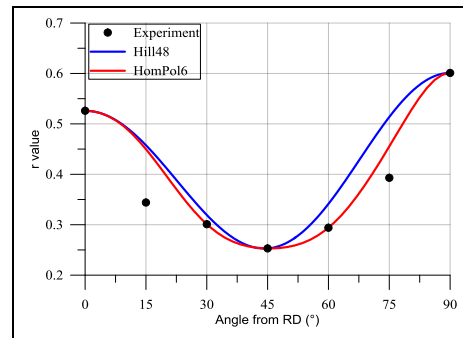


Figure 2. Yield surfaces predicted by Hill48 and HomPol6 criterion.



(a)



(b)

Figure 3. Directionalities of (a): Yield stress ratios and (b): Lankford coefficients predicted by Hill48 and HomPol6.

Both criteria reproduce elliptic and convex yield surfaces. The balanced biaxial yield stress value is an input for the HomPol6 criterion, whereas the r based Hill48 criterion does not include this data. Therefore, HomPol6 captured the balanced biaxial yield stress value contrary to the Hill48 criterion, as seen in Figure 2. In addition, HomPol6 captured both r values and yield stress ratios in all experimentally measured orientations. This improved prediction performance is based on the high number of anisotropy parameters. Nonetheless, the Hill48 criterion could only capture the r values in RD, DD, and TD, since Hill48 has six anisotropy parameters, and only four of them are relevant to the in-plane anisotropy features. A yield criterion should successfully predict both r value and yield stress ratio directionalities for an accurate earing defect prediction in a cup

drawing process. The r values are essential for capturing the maximum cup height location, while the magnitude of the ear is associated with the directional dependency of the yield stress ratio. In this regard, the HomPol6 criterion was seen to be more efficient compared to the Hill48 criterion.

The drawing simulations of AA6016-T4 aluminum alloy were conducted based on the isotropic hardening rule and combined hardening rule separately so as to show the pure influence of the combined hardening rule. Therefore, the parameters belonging to the isotropic and combined hardening rule assumptions were obtained by using the curve fitting method. The rolling direction (RD) was regarded as the reference direction to the hardening parameter's determination, and The Levenberg – Marquardt algorithm was adopted in MATLAB Curve Fitting Tool. The Swift law was assumed (Eq. (30)) for the hardening characterization, and the hardening parameters for only isotropic hardening rule assumption were summarized in Table 4. Figure 4 shows the generated flow curve.

$$\sigma_{true} = K(\epsilon_0 + \epsilon_p)^p \quad (30)$$

Table 4. Hardening curve parameters of AA6016-T4.

	K [MPa]	p	ϵ_0
Swift Law	474.1	0.2703	0.002299

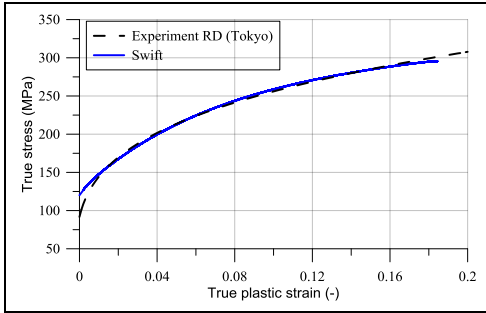


Figure 4. Hardening curve of AA6016-T4.

The reversal shear test data provided by the ESAFORM benchmark organizers were employed to obtain the combined isotropic-kinematic hardening parameters [16]. To this end, a representative unit volume element (RVE) was utilized, and inverse method was adopted. Reversal shear test conditions were applied to the RVE (Figure 5). By adjusting the kinematic and isotropic hardening parameters simultaneously, the reversal behavior of the material was tried to be estimated.

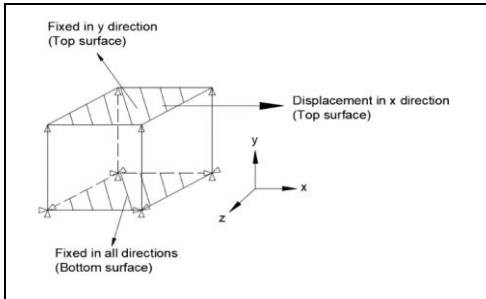


Figure 5. Reversal shear boundary conditions on RVE.

The total hardening curve equals the sum of the reference yield stress, isotropic hardening, and back stress curves. The mathematical expression of the total hardening curve was given in Eq. (31).

$$\sigma = \sigma_r + \frac{Q}{b}(1 - e^{-b\epsilon^p}) + \frac{C}{\gamma}(1 - e^{-\gamma\epsilon^p}) \quad (31)$$

Here, the second and the third terms on the right side of the expression represent isotropic hardening and back stress (kinematic hardening), respectively. Correspondingly, Q and b are associated with isotropic hardening, while C and γ are associated with the back stress curve. Table 5 summarizes the combined hardening parameters. In addition, Figure 6 demonstrates the predicted isotropic hardening and back stress curves.

Table 5. Combined isotropic-kinematic hardening rule parameters of AA6016-T4.

σ_{ref} [MPa]	Q	b	C	γ
71	1490	7.4	15000	166.66

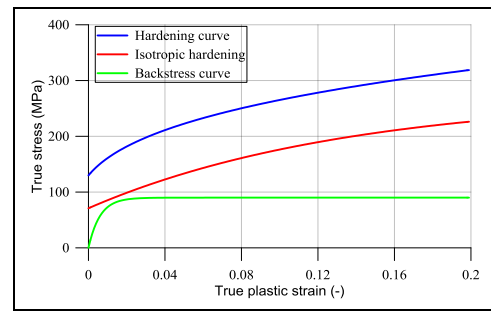


Figure 6. Reversal shear boundary conditions on RVE.

5 Cup drawing simulations

The drawing process was analyzed in implicit Marc software coupled with the Hypela2 user-defined material subroutine. Blank was discretized with full integration constant dilatational hexahedral elements (Hex7 in Marc software), which are free from shear locking [35],[36]. In through-thickness direction, blank was meshed with two elements. The process tools except for the blank were assumed as geometric surfaces, and control nodes were assigned to the blank holder and punch to define the force and displacement boundary conditions. Rigid body stoppers were also modeled using solid rigid elements. Figure 7 illustrates the FE model of the cup drawing process and the generated mesh layout.

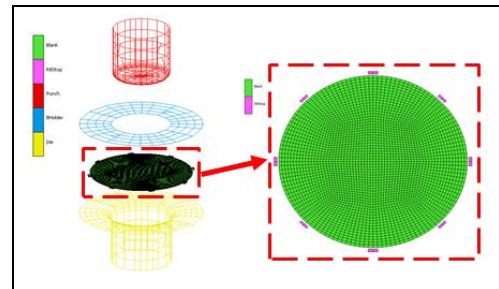


Figure 7. FE model of the cup drawing process.

The coefficient of friction between the blank and the other tools was assumed to be 0.1, and the Coulomb bilinear friction type was assumed. A segment-to-segment contact algorithm with the Lagrangian multiplier method was adopted to minimize the penetration. A clamping force of 40 kN was acted on the blank, and the simulations were suspended when the punch moved about 54 mm.

6 Results

The punch force-displacement responses and the ear formation results predicted by Hill48 and HomPol6 criteria were presented in this section. Initially, the prediction results based on the isotropic hardening rule were presented. Later, the results obtained from the combined isotropic-kinematic hardening rule assumption were illustrated to show the improvement in the prediction performance.

Most of the participants of the ESAFORM 2021 benchmark study [16] encountered the ironing issue in their analyses. Besides, the wearing on the die radius region was also pointed out and the clearance at the cup wall (between the punch and die surfaces) was reported to be higher than initially depicted value. Therefore, the clearance at the cup wall region was increased from 1.2 mm to 1.4 mm in the simulations so as to demonstrate the capability of the implemented plasticity models. In the first stage, the cylindrical cup drawing analyses were carried out for Hill48 and HomPol6 yield criteria considering only the proportional expansion of the yield surface (isotropic hardening). The punch force-displacement and earing profile predictions based on the isotropic hardening rule assumption were demonstrated in Figure 8.

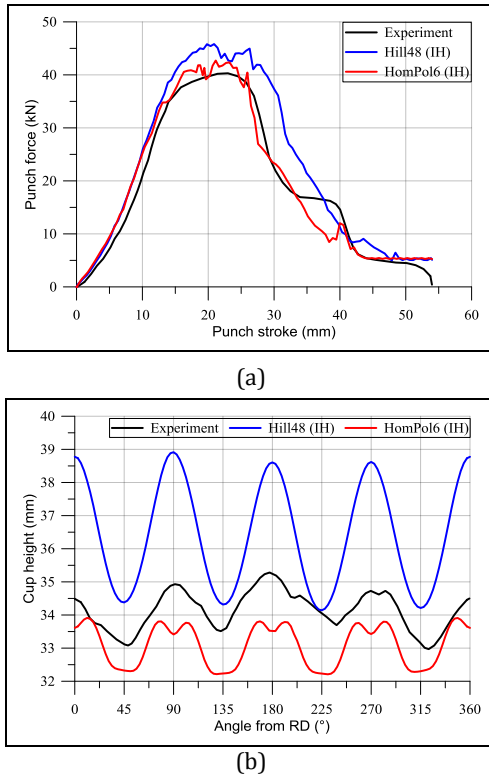


Figure 8(a): Punch force-stroke. (b): Earing profile results obtained by Hill48 and HomPol6 criteria based on isotropic hardening (IH) rule assumption.

The HomPol6 criterion showed better agreement than the Hill48 criterion for both punch force-stroke and earing profile predictions. Hill48 criterion overpredicted the punch force response, while HomPol6 estimated the punch force with high accuracy. Besides, Hill48 predicted higher earing amplitude and cup height values when compared to both the experimental response and HomPol6. On the other hand, both criteria captured the maximum cup height locations successfully. The combined hardening rule was assumed in the second stage, and

the analyses were repeated for both yield criteria. Figure 9 presents the punch force-stroke response and comparative earing profile predictions.

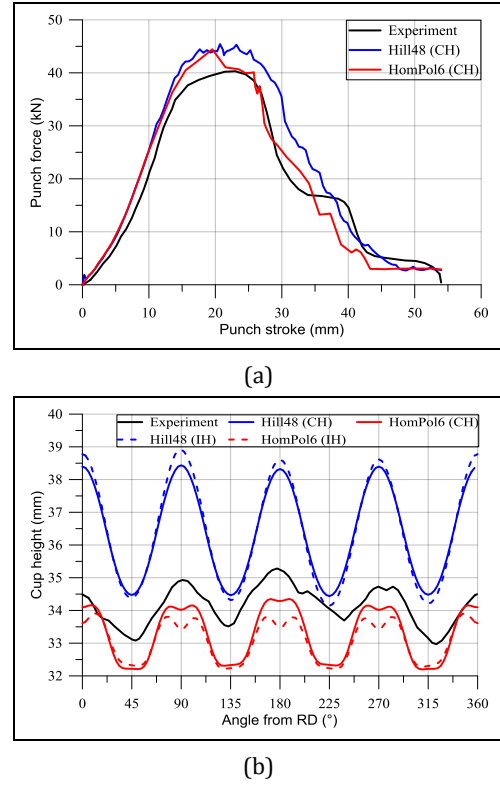


Figure 9. Comparison of (a): Punch force-stroke. (b): Earing profile results of Hill48 and HomPol6 based on isotropic combined hardening rules.

Two yield criteria in conjunction with the combined hardening rule led to reasonable punch force-displacement predictions that are consistent with the experimental outcomes. On the other hand, whether the combined hardening effect was incorporated into the analyses, the trends of the punch force-stroke response predictions for both yield criteria were not changed dramatically. Only slight differences between the assumptions of isotropic hardening and combined hardening were observed in the punch force-stroke predictions. Othmen et al. [11] also lay emphasis on the same outcome.

As regards the prediction of ear formation, a significant enhancement was observed in the numerical results. With the combined hardening effect, the cup height results converged to the experimental earing profile. These outcomes are also in line with the results of Chatti and Chtioui [8]. They conducted a similar study on a different aluminum alloy, and they observed an improvement in the earing profile predictions when the kinematic hardening effect was included. However, the improvement in HomPol6 was more apparent compared to the Hill48 criterion. The earing amplitude is slightly decreased for Hill48, whereas distinctively increased HomPol6 coupled with combined hardening rule showed the best agreement. In addition, at the vicinity of 270° degrees, two ears were observed in the physical test, which is captured by the HomPol6 criterion accurately.

7 Summary and conclusions

The present study evaluates the influence of combined isotropic-kinematic hardening model coupled with the

quadratic Hill48 and the HomPol6 yield criteria on the prediction of ear formation after a cup drawing operation. The combined hardening model regarded the effect of the bending-unbending issue observed at the punch and die radius on the earing prediction. Besides, the HomPol6 employed for the accurate yield surface description is an advanced yield criterion with 16 adjustable parameters that capture the biaxial data as well as the r value and yield stress change with respect to the different material orientations. On the other hand, the Hill48 criterion is a fundamental function and was adopted for only comparison purposes. An anisotropic metallic material, namely AA6016-T4 aluminum alloy was used as a test material. The aforementioned yield criteria and the combined hardening model were implemented into the Hypela2 user-defined subroutine. The kinematic component of the combined hardening model was characterized by the Armstrong-Frederic nonlinear hardening model. In the first stage of the study, only the isotropic hardening rule was assumed, then the simulations were repeated with combined isotropic – kinematic hardening assumption. For both cases, the punch force – stroke and cup height-the angle from RD responses were numerically measured, and these responses were compared with the experimental outcomes. Conclusions drawn from present study are as follows.

- ✓ The HomPol6 criterion successfully predicted the anisotropic response of the AA6016-T4 aluminum alloy. Furthermore, the HomPol6 criterion could capture the biaxial yield stress ratio and provide a proper yield locus description. However, the Hill48 criterion could only capture the r values in RD, DD, and TD. The balanced biaxial yield stress and the directional dependency of the yield stress ratio could not be predicted by Hill48,
- ✓ The experimental punch force-stroke responses were accurately predicted by both isotropic hardening and combined hardening rules coupled with HomPol6. Although there are minor differences between them, the general trendlines of the punch force-stroke responses were similar to each other. Whether the combined hardening rule was assumed or not, the Hill48 criterion estimated higher earing amplitude in comparison to the HomPol6 and experimental profile,
- ✓ With the inclusion of the combined hardening, the earing profile prediction performance was noticeably increased for the HomPol6. However, a striking improvement was not observed in the Hill48 predictions. The mean cup height values and the magnitude of the ears were simultaneously increased for HomPol6, while only the earing magnitude was slightly decreased for Hill48,
- ✓ It was seen that an advanced yield criterion coupled with a combined hardening model is highly essential for an improved earing prediction performance.

8 Author contribution statement

In the present study, Toros Arda AKŞEN took part in the literature review, performing the analyses, writing the original draft, collecting data. Murat ÖZSOY contributed to the writing-review editing, methodology, visualization, Mehmet FIRAT contributed to the methodology, conceptualization, supervision.

9 Ethics committee approval and conflict of interest statement

There is no need for any permission from ethics committee for the article prepared.

The authors declare that they have no conflict of interest for the article prepared.

10 References

- [1] Köksal NS, Uzkut M. "Determination of formability parameters of Erdemir 6114 sheets tempered at dual phase regions". *Pamukkale University Journal of Engineering Sciences*, 7(3), 337-341, 2001.
- [2] Chung K, Shah K. "Finite element simulation of sheet metal forming for planar anisotropic metals". *International Journal of Plasticity*, 8, 453-476, 1992.
- [3] Yoon JW, Barlat F, Chung K, Pourboghraat F, Yang DY. "Influence of initial back stress on the earing prediction of drawn cups for planar anisotropic aluminum sheets". *Journal of Materials Processing Technology*, 80-81, 433-437, 1998.
- [4] Yoon JW, Barlat F, Chung K, Pourboghraat F, Yang DY. "Earing predictions based on asymmetric nonquadratic yield function". *International Journal of Plasticity*, 16, 1075-1104, 2000.
- [5] Yoon JW, Barlat F, Dick RE, Karabin ME. "Prediction of six or eight ears in a drawn cup based on a new anisotropic yield function". *International Journal of Plasticity*, 22, 174-193, 2006.
- [6] Yoon JH, Cazacu O, Yoon JW, Dick RE. "Earing predictions for strongly textured aluminum sheets". *International Journal of Mechanical Science*, 52, 1563-1578, 2010.
- [7] Vladimirov IN, Schwarze M, Reese S. "Earing prediction by a finite strain multiplicative formulation for anisotropic elastoplastic materials". *GAMM Mitteilungen*, 33, 116-129, 2010.
- [8] Chatti S, Chtioui N. "Sheet metal forming simulation using finite elastoplasticity with mixed isotropic/kinematic hardening". *European Journal of Computational Mechanics*, 20, 427-453, 2011.
- [9] Vrh M, Halilovic M, Starman B, Stok B, Comsa DS, Banabic D. "Capability of the BBC2008 yield criterion in predicting the earing profile in cup deep drawing simulations". *European Journal of Mechanics A/Solids*, 45, 59-74, 2014.
- [10] Park T, Chung K. "Non-associated flow rule with symmetric stiffness modulus for isotropic-kinematic hardening and its application for earing in circular cup drawing". *International Journal of Mechanical Sciences*, 115-116, 553-563, 2016.
- [11] Othmen KB, Sai K, Manach PY, Elleuch K. "Reverse deep drawing process: Material anisotropy and work-hardening effects". *Journal of Materials: Design and Application*, 233, 699-713, 2019.
- [12] Grillo TJ, Valente RAF, Alves de Souza RJ. "Modelling non-quadratic anisotropic yield criteria and mixed isotropic-nonlinear kinematic hardening: analysis of forward and backward-Euler formulations". *International Journal of Material Forming*, 8, 533-547, 2015.
- [13] Izadpanah S, Ghaderi SH, Gerdooei M. "Material parameters identification procedure for BBC2003 yield criterion and earing prediction in deep drawing". *International Journal of Solids and Structures*, 49, 3582-3593, 2012.

- [14] Singh A, Basak S, Prakash L, Roy GG, Jha MN, Mascarenhas M, Panda SK. "Prediction of earing defect and deep drawing behavior of commercially pure titanium sheets using CPB06 anisotropy yield theory". *Journal of Manufacturing Processes*, 33, 256-267, 2018.
- [15] Feng Z, Yoon SY "Prediction of earing defect and deep drawing behavior of commercially pure titanium sheets using CPB06 anisotropy yield theory". *Journal of Manufacturing Processes*, 33, 256-267, 2018.
- [16] Habraken AM, Akşen TA, Alves JL, et al. "Analysis of ESAFORM 2021 cup drawing benchmark of an Al alloy, critical factors for accuracy and efficiency of FE simulations". *International Journal of Material Forming*, 15, 1-96, 2022.
- [17] Kim J, Pham QT, Ha J, Kim YS. "Constitutive modeling of commercial pure titanium sheet based on non-associated flow rule and differential hardening". *International Journal of Mechanical Sciences*, 230, 1-17, 2022.
- [18] Taherizadeh A, Green DE, Ghaei A, Yoon JW. "A non-associated constitutive model with mixed iso-kinematic hardening for finite element simulation of sheet metal forming". *International Journal of Plasticity*, 26, 288-309, 2010.
- [19] Mendiguren J, Rolfe B, Weiss M. "On the definition of an kinematic hardening effect graph for sheet metal forming process simulations". *International Journal of Mechanical Sciences*, 92, 109-120, 2015.
- [20] Prager W. "A new method of analyzing stresses and strains in work hardening plastic solids". *ASME Journal of Applied Mechanics*, 23, 493-496, 1956.
- [21] Ziegler HA. "A modification of Prager's hardening rule". *Quarterly of Applied Mechanics*, 17, 55-65, 1959.
- [22] Besseling JF. "A theory of plastic and creep deformations of an initially isotropic material". *ASME Journal of Applied Mechanics*, 25, 529-536, 1958.
- [23] Mroz Z. "On the description of anisotropic work hardening". *Journal of Mechanics and Physics of Solids*, 15, 163-175, 1967.
- [24] Dafalias YF, Popov EF. "Plastic internal variables formalism of cyclic plasticity". *ASME Journal of Applied Mechanics*, 98, 645-651, 1976.
- [25] Armstrong PJ, Frederic CO. "A Mathematical Representation of the Multiaxial Bauschinger Effect". Scientific Report, G.E.G.B. Report RD/B/N, Scientific Report, 731, 1966.
- [26] Ohno N, Wang JD. "Kinematic hardening rules with critical state of dynamic recovery. Part 1: Formulations and basic features for ratcheting behavior". *International Journal of Plasticity*, 9, 375-390, 1993.
- [27] Yıldız H, Kırılı O. "Non-linear finite element modeling of deep drawing process". *Pamukkale University Journal of Engineering Sciences*, 10(3), 317-326, 2004.
- [28] Hill R. "A theory of the yielding and plastic flow of anisotropic metals". *Proceeding of the Royal Society London A*, 193A, 291-297, 1948.
- [29] Gotoh M. "A theory of plastic anisotropy based on a yield function of fourth order (plane stress state)". *International Journal of Mechanical Sciences*, 19, 505-512, 1977.
- [30] Soare S, Yoon JW, Cazacu O. "On the use of homogeneous polynomials to develop anisotropic yield functions with applications to sheet forming". *International Journal of Plasticity*, 24, 915-944, 2008.
- [31] Soare SC. On the Use of Homogeneous Polynomials to Develop Anisotropic Yield Functions with Applications to Sheet Forming. PhD Thesis, University of Florida, Florida, USA, 2007.
- [32] Firat M. (2008) "A numerical analysis of sheet metal formability for automotive stamping applications". *Computational Materials Science*, 43, 802-811, 2008.
- [33] Paul SK, Sivaprasad S, Dhar S, Tarafder M, Tarafder S. "Simulation of cyclic plastic deformation response in SA333 C-Mn steel by a kinematic hardening model". *Computational Materials Science*, 48, 662-671, 2010.
- [34] Zang SL, Guo C, Thuillier S, Lee MG. "A model of one surface cyclic plasticity and its application to springback prediction". *International Journal of Mechanical Sciences*, 53, 425-435, 2011.
- [35] MSC. Software Corporation. "Volume A: Theory and User Information". <https://simcompanion.hexagon.com/customers/s/article/msc-marc-volume-a--theory-and-user-information-doc9245> (27.10.2023).
- [36] MSC. Software Corporation. "Volume B: Element Library". <https://simcompanion.hexagon.com/customers/s/article/volume-b--element-library-doc9246> (27.10.2023).